Study of Transient Laser-Induced Self-Focusing and Optical Modulation of Porous Silicon Films Using Pump-Probe Spectroscopy

Ammar T. Zakar [1]
Zeina T. AbdulRahman [2]
Thoalfiqar A. Zaker [3]

[1] *Department of Physics, College of Education for Pure Sciences, University of Mosul, Mosul, IRAQ*
[2] *Electrical Techniques, Technical Institute of Mosul, Northern Technical University, Mosul, IRAQ*
[3] *Department of Laser and Spectroscopy, Laser and Photonics Center, University of Al-Hamdaniya, Nineveh, IRAQ*

The transient transmittance change of microprous silicon was measured using optical pump – Mid infrared probe technique at different laser fluences. The results confirmed the existence of self-focusing in such structures at small incident angles and proper laser flounce. The measurements indicated that the self-focusing is not a long process which lasts for a short period of time. The tuneable focusing of MIR probe can be achieved with no need of adding any additional inclusions to the sample. This in turn provides the ability of sharpening or de-sharpening the profile of the probe beam. This also enables the utilization of such structures in the realm of stimulated depletion microscopy. The optical modulation change is also investigated based on Maxwell Grannet model. The model showed that the optically generated charge carriers increase with increasing the pumping fluence allowing the use of such structures as a tuneable optical modulator.

Keywords: Microporous silicon; Self focusing; Thermal lensing; Optical modulation
Received: 14 July 2024; Revised: 18 September; Accepted: 25 September 2024

1. Introduction

Many unintuitive phenomena occur when light propagates through a nonlinear medium. The importance of these effects in different applications has made them a major topic for many research groups. These effects play a key role in various applications such as imaging, polarization control and phase matching [1-7] . Most of these phenomena are due to the fact that the refractive index of the substances depends on the intensity of the incident light. Some of these effects become significant at high energy ultrashort laser pulses while this is not the case with composite materials (optically anisotropic materials). The ability of such materials to shape the propagation of light is due to the change in their refractive indices (birefringence). The propagation of light causes some unwanted optical effects such as sample damaging through self-focusing as well as two photon absorption. However, some of these effects could be useful in the field of all optical switching [8] and 3d laser micro-structuring [9]. Structured nanocomposites represent an additional category of birefringent materials, their anisotropic properties can be derived from inclusions of a secondary material at the nanometer scale [10-12]. However, changing the anisotropic properties and in turn the birefringent behavior for most of the composites is not an easy process as the preparation and incorporation of inclusions within the structure are quiet challenging. Some silicon derivative materials such as porous silicon and porous silicon oxide ($PSiO_2$) are mesoporous composites with birefringence resulting from their extremely uneven pore structure [13-17]. The optical properties and birefringence of the porous silicon are significantly affected by presence of inclusions and its size distribution [18,19]. This can result in widely recognized occurrences of self-phase modulation and self-focusing [20]. In the case of porous silicon, both refractive index and birefringence can be modified during the fabrication process. This gives the possibility of producing elements with gradient refractive index by varying the current during the etching process [21-23]. The birefringence of porous silicon is also significantly affected by changing the porosity and can reaches values greater than 0.3 at visible spectrum [16]. This can be exploited in the fabrication of dielectric mirrors and birefringent spectral filters where the produced elements can focus or defocus the light depending on the polarization state of the incident beam [24,25]. However, predicting the lensing and polarization sensitivity behaviour of such structures is difficult and needs more thorough investigation. The change in the refractive index can be achieved either by adjusting the etching conditions during the fabrication process or through the external excitation of the sample. The absorption of the excited beam

generates thermal gradient refractive index around the excited area. The generated thermal gradient acts as a thermal lens and the related changes in the transmitted beam depends on the degree of the lens. This behaviour can be exploited in different optical compounds as the degree of the lens can be simply controlled by appropriate selection of the excited wavelength [26,27]. The effect of thermal lensing was first observed by Gordon et al, since then many optical configurations and theoretical models have been proposed to improve the sensitivity and the analysis of the detected signal [28].

The aim of this study involves the evaluation of the transient self-focusing and optical intensity modulation of microporous silicon. The focusing behaviour is extremely important in the investigation of under surface imaging of silicon and silicon derivative materials depending on the wavelength and pulse duration of the pump beam. This also provides the ability of sharpening or de-sharpening the profile of the probe beam, which in turn plays a significant role in the development of stimulated depletion microscopy.

2. Experimental Part

The porous silicon film was fabricated based on the photo-electrochemical etching of silicon wafer in HF. The surface of the sample contains a well arranged pores with a diameter rang of 0.9-1 µm. The pores are separated by 1.5 µm pitch on square pattern as shown in Fig. (1a). The arrangement of pores as well as the inter-pore distance (thickness of 15 µm) are determined by a pre-structured photo mask. More details about the fabrication process can be found elsewhere [29].

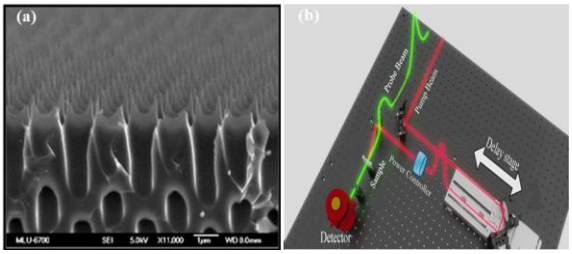

Fig. (1) (a) The cross section surface of microporous silicon. The structure encompasses well-arranged pores with diameter of 0.9-1 µm and pitch of 1.5 µm (b) the optical setup

The time resolved transmittance was measured using Coherent laser system based on optical pump – MIR probe approach as shown in the Fig. (1b). The system provides a laser beam with average power of 3.2 W, 800 nm wavelength, 60 fs pulse duration and 1khz repetition rate respectively. The emerged beam was split into two components: the first component was guided to optical parametric amplifier (OPA) to generate 4 µm probe wavelength, while the second component is used as a pumping source. The time delay between both beams was controlled using retro reflector attached to motorized translation stage. A combination of polarizer and half wave plate were used to control the pumping power. The incident angle of the pump and probe signals was fixed at 10° and 5° with respect to the normal to the surface. The polarization of the pump and probe beams was perpendicularly oriented to avoid any interference. The knife edge technique was employed to measure the spot size for both beams which found to be 623 µm for the pump and 200 µm for the probe respectively. The InSb thermal detector was used to measure the intensity of the transmitted probe signal.

3. Results and Discussions

Figure (2) shows the transient transmittance change at different pumping powers, ranging from 10 to 50 mW corresponding to peak fluences ranging from 5.68 to 28.41 mJ/cm^2. The transmittance change follows the same behaviour for all pumping powers where the intensity increases at time delay t=0 between the pump and probe signals followed by a decrease.

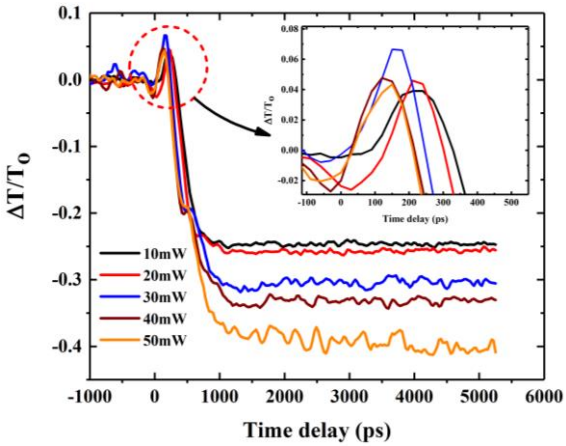

Fig. (2) (a) The transient transmittance of 15µm microporous silicon measured based on optical pump (800nm), MIR probe (4µm) at different excitation levels. The insect indicates the zoomed self-focusing peaks

The incident pump generates both temperature distribution around the excited area and surface deformation depending on many parameters such as polarization state, wavelength, pulse duration and focusing of the excited pulse. Thus, the increase in transmittance is due to plasma dispersion effect generated by the pump. In this process, the absorption of the pump signal by free carriers leads to the generation of donut like distribution of free carriers as shown in Fig. (3). Accordingly, The generated distribution yields thermal gradient refractive index (lower refractive in the centre compared to the edge of the donut). This in turn acts as a dynamical lens focusing or defocusing the probe beam depending on the excitation fluence. Some studies suggested that the focusing and defocusing of the probe beam can be controlled based on the shape of the excitation pulse, where the Gaussian like pump yields defocusing of the probe beam while the donut like produces focusing behaviour [30]. Other study

attributed the self-focusing effect to the structure induced nonlinearity in which the free carriers have no direct contribution [31].

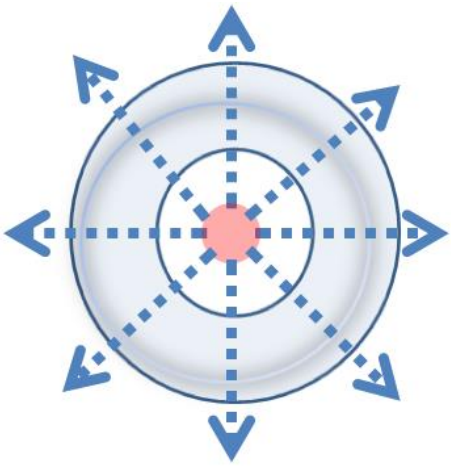

Fig. (3) The donut like distribution of free carriers generated by the pump beam

The intensity of the transmitted probe can be either sharpened or de-sharpened by changing the pumping power or through fine tuning the time delay between the pump and probe beams as observed in Fig. (2). This figure also revealed that the self-focusing behaviour lasts for specific time delay between the pump and probe beams. The decrease in the transmittance following the self-focusing process is a well-known trend of the porous silicon which results from free carrier absorption[30]. It's worth mentioning that the focusing behaviour can be only observed at incident angles close to the normal for both pump and probe beams as the excitation becomes more distributive at larger angles with respect to the normal.

Figure (4) shows the maximum self-focusing peak intensity of micro porous silicon at different pumping powers. The figure revealed that the focusing becomes more intense at some specific pumping fluences followed by degradation at higher excitations as the free carrier absorption dominates the process.

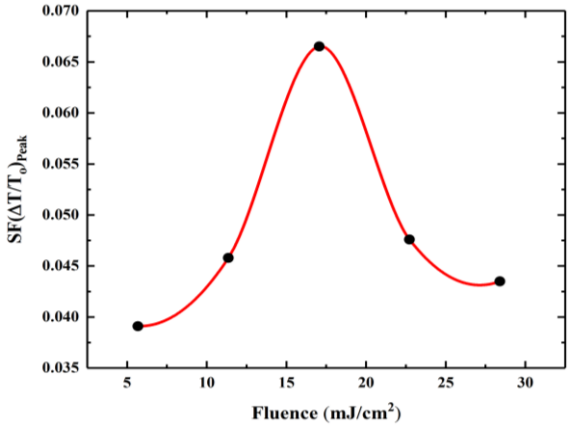

Fig. (4) The self-focusing maximum intensity of the peaks as a function at pump fluencies ranging from 5.68 to 28.41 mJ/cm^2

To estimate the temperature evolution of the excited area, the solution of the following heat equation is used with some specific consideration:

$$c\rho\frac{\partial}{\partial t}[\Delta T(r,t)] = \dot{g} + k\Delta^2[\Delta T(r,t)] \qquad (1)$$

where c , ρ , g, k represent heat capacity, the density of the sample, the source term and the thermal conductivity, respectively

The solution of the above equation for the boundary conditions $(r < \infty)$ and $(\Delta T(r,0) = 0)$ can be expressed as follows:

$$\Delta T(r,t) = \frac{0.24P\alpha}{4\pi k}\left\{\ln\left(1+\frac{2t}{\tau_c}\right) + \sum_{n=1}^{\infty}\frac{(\frac{-2r^2}{\omega^2})^n}{nn!}\times\left[1-\left(\frac{1}{1+\frac{2t}{\tau_c}}\right)^n\right]\right\} \qquad (2)$$

where P , α , r, ω , t , τ_c refer to laser power, absorption coefficient, radius of the beam with respect to the axis, radius of the pump beam, time delay between the pump and probe signals and the build-up time of the lens, respectively. The average build-up time values (140, 93, 105, 148, and 161 ps) were extracted from Fig. (2). The above equation can be employed to calculate the temperature evolution as a function of spot size and time respectively. As the size of the pump is constant, the equation becomes time dependent only at different excitation levels. The temperature change of the excited porous silicon film during the build-up lensing time is shown in Fig. (5). The build-up time of the self-focusing is short at low pumping fluencies compared to higher excitations as the contribution of the carriers absorption starts to dominate the process. Based on the calculated temperature values, the change in the refractive index can be also calculated using the following equation:

$$n(t) = n_o - \frac{dn}{dT}\Delta T(t) \qquad (3)$$

where n_o is the intial refractive index and $\frac{dn}{dT}$ refers to the temperature coefficient of the silicon

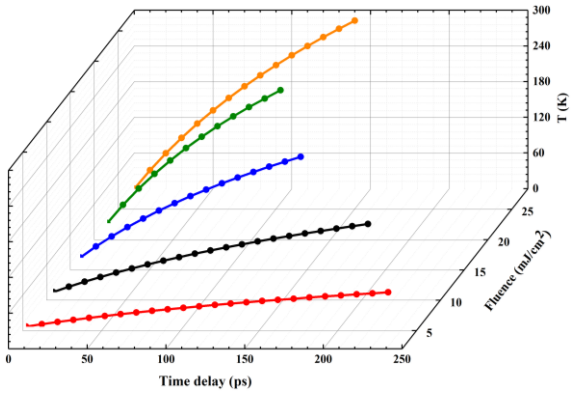

Fig. (5) The transient building up temperature of the excited sample at different pumping levels

Figure (6) shows the time resolved refractive index during the build-up time of the self-focusing at different pumping powers. It can be seen from the figure that the refractive index decreases with the

increase in the pumping power. The results also indicates that the pump produces donut like plasma dispersion with lower refractive index in the centre of the excitation area compared to the edge of the donut. Thus, the increase in transmittance intensity is due to the relative decrease in the refractive index.

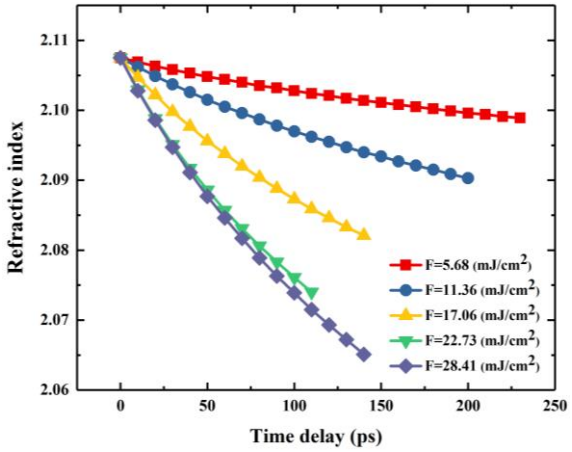

Fig. (6) The time-dependent refractive index calculated based on the temperature evolution of the excited sample

The probe intensity modulation as well as the contribution of the carrier concentration following the self-focusing can be evaluated using Maxwell Grannet approximation together with Drude model as expressed in the following equations:

$$\varepsilon_{eff}^{o} = \varepsilon_m \frac{2f(\varepsilon_i-\varepsilon_m)+\varepsilon_i+2\varepsilon_m}{2\varepsilon_m+\varepsilon_i-f(\varepsilon_i-\varepsilon_m)} \quad (4)$$

where f , ε_m , ε_i represent the volume fraction, dielectric constant of the matrix and the dielectric constant of the inclusion, respectively

The Drude contribution can be expressed as:

$$\Delta\varepsilon = \frac{\omega_P^2}{\omega^2+i\gamma\omega} \quad (5)$$

$$\omega_P^2 = \frac{e^2N}{\epsilon_o m_e m^*} \quad (6)$$

Here, ω_P^2 , ω represent the plasma and the probe frequencies, respectively, and γ refers to the scattering rate with N, ϵ_o, m_e and m^* are the carrier concentration, permittivity, electron mass and effective electron mass, respectively

The incorporation of the Drude model into Maxwell Garnett approximation can be expressed as follows:

$$\varepsilon_{eff} = \varepsilon_{eff}^{o} - \Delta\varepsilon \quad (7)$$

Figure (7) shows the maximum transmittance change as a function of the pumping fluence. It can be observed from the figure that the transmittance degrades as the excitation increases indicating that the sample becomes rather absorptive at higher exaction levels. Based on that the carrier concentration of the excited film can be extracted by fitting the Maxwell Garnett model to the maximum transmittance change following the self-focusing process as shown in Fig. (8). This figure indicated that the carrier generation enhances as the pump fluence increases. It should be mentioned here that the nature of the carrier scattering in the excited sample cannot be revealed directly based on Drude model only. Thus, the scattering rate is assumed to be constant during the fitting process and its value is fixed around $1x10^{-5}$ s^{-1}. The fitting process provides the possibility of extracting the complex dielectric function at maximum transmittance change as a function of pumping fluence as shown in Fig. (9).

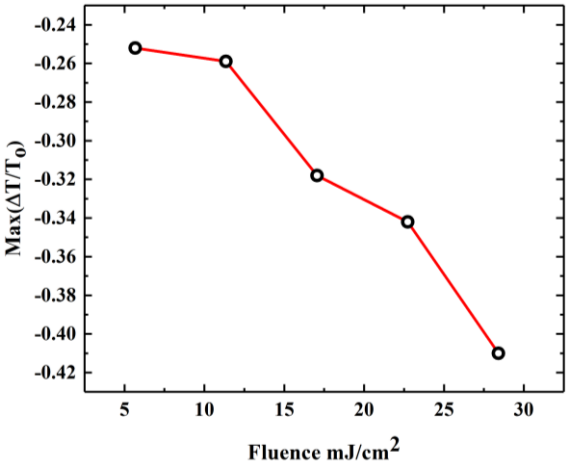

Fig. (7) The maximum transmittance change as a function of pumping fluence

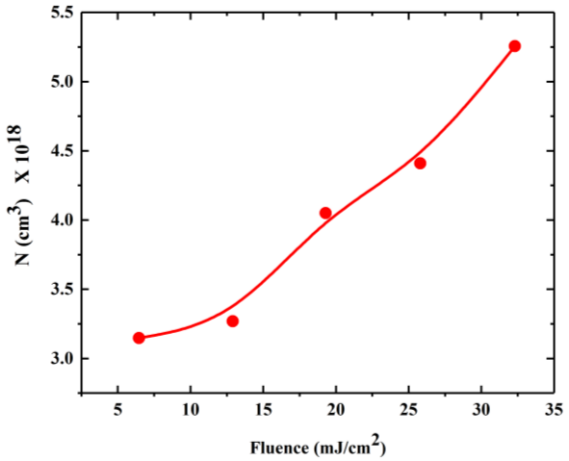

Fig. (8) The carrier concentration of the excited sample extracted using Maxwell Garnett model modified to involve Drude model

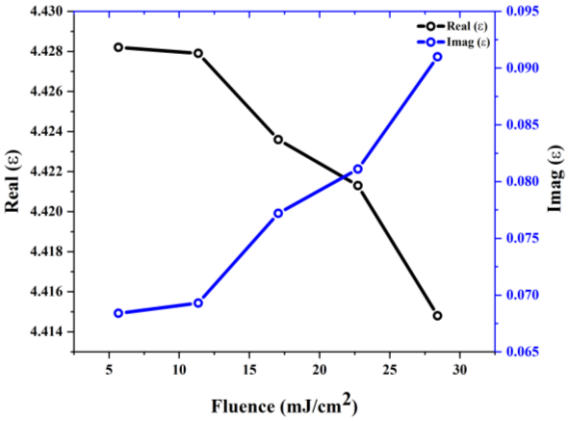

Fig. (9) The real and imaginary parts of the complex dielectric function estimated using MG model together with Drude like contribution

Figure (9) shows the fluence dependent real and imaginary parts of the dielectric function of the excited film extracted using above mentioned model. As can be seen, the real part degrades with increasing the excitation fluence due to the change in the optical properties of the film induced by the pumping pulse. In contrast, the imaginary part of the dielectric function increases with increasing the excitation fluence. This in turn indicates that the sample turns out to be more absorptive at high pumping levels.

4. Conclusion

The results indicated that the self-focusing lasts for specific delay time between the pump and probe signals. The results also revealed that the self-focusing can be only observed at incident angles close to the normal. The time resolved measurements revealed lensing build up times of 140, 93, 105, 148, and 161 ps at different pumping fluencies. The peak intensity of lensing can be controlled either by the pump fluence or through changing the time delay between the pump and probe signals. The Maxwell Grannet model revealed an enhancement in the carrier concentration with increasing the pumping power providing the possibility of using such structures as tuneable optical modulator where the intensity of the probe can be controlled optically.

References

[1] M.F. Weber et al., "Giant birefringent optics in multilayer polymer mirrors", *Science*, 287(5462) (2000) 2451-2456.

[2] M. Beresna, M. Gecevičius, and P. G. Kazansky, "Polarization sensitive elements fabricated by femtosecond laser nanostructuring of glass", *Opt. Mater. Exp.*, 1(4) (2011) 783-795.

[3] J.A. Davis, I. Moreno and P.J. Tsai, "Polarization eigenstates for twisted-nematic liquid-crystal displays", *Appl. Opt.*, 37(5) (1998) 937-945.

[4] J. Craven-Jones et al., "Infrared hyperspectral imaging polarimeter using birefringent prisms", *Appl. Opt.*, 50(8) (2011) 1170-1185.

[5] K. Oka and T.J. Kaneko, "Compact complete imaging polarimeter using birefringent wedge prisms", *Opt. Exp.*, 11(13) (2003) 1510-1519.

[6] Y. Yasuno et al., "Birefringence imaging of human skin by polarization-sensitive spectral interferometric optical coherence tomography", *Opt. Lett.*, 27(20) (2002) 1803-1805.

[7] C.K. Park, S. Lee and Y.S. Hwang, "Depth-extended integral imaging system based on a birefringence lens array providing polarization switchable focal lengths", *Opt. Exp.*, 17(21) (2009) 19047-19054.

[8] J.J. Qiu, "Femtosecond laser-induced microstructures in glasses and applications in micro-optics", *The Chem. Record*, 4(1) (2004) 50-58.

[9] D. Ashkenasi et al., "Application of self-focusing of ps laser pulses for three-dimensional microstructuring of transparent materials", *Appl. Phys. Lett.*, 72(12) (1998) 1442-1444.

[10] M.S. Rill et al., "Negative-index bianisotropic photonic metamaterial fabricated by direct laser writing and silver shadow evaporation", *Opt. Lett.*, 34(1) (2009) 19-21.

[11] A. Lutich et al., "Birefringence of nanoporous alumina: dependence on structure parameters", *Appl. Phys. B*, 84 (2006) 327-331.

[12] T.J. Takamori, "Structural anisotropy and birefringence in microporous glasses", *J. Amer. Cer. Soc.*, 61(9-10) (1978) 434-438.

[13] L. Canham, **"Handbook of Porous Silicon"**, Springer Int. Pub. (Berlin, 2014), pp. 133-149.

[14] V.Y. Timoshenko et al., "Anisotropy of optical absorption in birefringent porous silicon", *Phys. Rev. B*, 67(11) (2003) 113405.

[15] O. Sarbey et al., "Birefringence of Porous Silicon", *Phys. Solid State*, 42(7) (2000) 1-2.

[16] K. Hakshur and S. J. Ruschin, "Observation of a large optical birefringence effect in a (110) oriented porous silicon layer", *Appl. Phys. Lett.*, 104(5) (2014) 2-3.

[17] L. Golovan, P. Kashkarov and V.Y. Timoshenko, "Form birefringence in porous semiconductors and dielectrics: a review", *Crystallog. Rep.*, 52 (2007) 672-685.

[18] S. Lettieri et al., "Nonlinear optical refraction of free-standing porous silicon layers", *Opt. Commun.*, 168(5-6) (1999) 383-391.

[19] Y.R. Shen, **"Principles of Nonlinear Optics"**, John-Wiley & Sons (NY, 1984), pp. 505-518.

[20] G.V. Prakash et al., "Nonlinear optical properties of silicon nanocrystals grown by plasma-enhanced chemical vapor deposition", *J. Appl. Phys.*, 91(7) (2002) 4607-4610.

[21] N.A. Krueger et al., "Porous silicon gradient refractive index micro-optics", *Nano Lett.*, 16(12) (2016) 7402-7407.

[22] T.J. Tibsibim and G.U. Jasbijn, "Characteristics of Tin Oxide Nanostructures Deposited on Porous Silicon Substrates", *Iraqi J. Mater.*, 2(4) (2023) 175-180.

[23] U.A. Merhan and T.B. Simanja, "Characterization of Cu_2S-Doped Nanostructured ZnS Thin Films Deposited on Porous Silicon", *Iraqi J. Mater.*, 3(1) (2024) 33-38.

[24] J. Álvarez et al., "Birefringent porous silicon membranes for optical sensing", *Opt. Exp.*, 19(27) (2011) 26106-26116.

[25] N. Shokoufi, A. Abbasi-Ahd and K.J. Kargosha, "Laser induced thermal lens microscopy for highly sensitive determination of captopril", *Appl. Opt.*, 56(11) (2017) E58-E63.

[26] T.J. Kitamori, "Thermal lens microscope and microchip chemistry", *Bull. Chem. Soc. Japan*, 92(2) (2019) 469-473.

[27] T. Le et al., "Detection of zeptomole quantities of nonfluorescent molecules in a 10nm

nanochannel by thermal lens microscopy", *Analyst*, 139(11) (2014) 2721-2725.
[28] M. Sabaeian and H.J. Nadgaran, "An analytical model for finite radius dual-beam mode-mismatched thermal lens spectroscopy", *J. Appl. Phys.*, 114(13) (2013)1-3.
[29] C. Levy-Clement et al., "Photoelectrochemical etching of silicon", *Electrochimica acta*, 37(5) (1992) 877-888.
[30] N. Shabairou et al., "Dynamics of laser-induced tunable focusing in silicon", *Sci. Rep.*, 12(1) (2022) 6342.
[31] R. Wu et al., "Active control of mid-wavelength infrared non-linearity in silicon photonic crystal slab", *Opt. Exp.*, 31(22) (2023) 35644-35652.
[32] A. Zakar et al., "Carrier dynamics and surface vibration-assisted auger recombination in porous silicon", *Phys. Rev. B*, 97(15) (2018) 155203.

